Research Article
DILI, Autoimmune, Cholestatic and Genetic Diseases

JOURNAL OF HEPATOLOGY

Beta-amyloid deposition around hepatic bile ducts is a novel pathobiological and diagnostic feature of biliary atresia

Graphical abstract

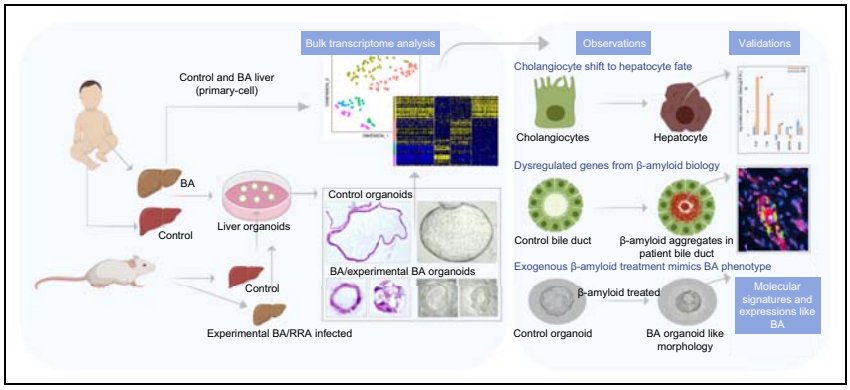

Highlights

- Liver organoids from patients with BA exhibited aberrant morphology and disturbed apical-basal organization.
- Transcriptomic analysis of BA organoids revealed a shift from cholangiocyte to hepatocyte transcriptional signatures.
- Beta-amyloid accumulation was observed around the bile ducts in BA livers.
- Exposure to beta-amyloid induced aberrant morphology in control organoids.
- Beta-amyloid accumulation represents a novel finding with pathobiological implications and diagnostic potential for BA.

Authors

Rosana Ottakandathil Babu, Vincent Chi Hang Lui, Yan Chen, …, Bin Wang, Urban Lendahl, Paul Kwong Hang Tam

Correspondence

szwb1967@126.com (B. Wang), urban.lendahl@ki.se (U. Lendahl), paultam@hku.hk (P.K.H. Tam).

Lay summary

Biliary atresia is a poorly understood and devastating obstructive bile duct disease of newborns. It is often diagnosed late, is incurable and frequently requires liver transplantation. Using human and mouse 'liver mini-organs in the dish', we unexpectedly identified beta-amyloid deposition – the main pathological feature of Alzheimer's disease and cerebral amyloid angiopathy – around bile ducts in livers from patients with biliary atresia. This finding reveals a novel pathogenic mechanism that could have important diagnostic and therapeutic implications.

https://doi.org/10.1016/j.jhep.2020.06.012
 J. Hepatol. 2020, 73, 1391–1403

Research Article
DILI, Autoimmune, Cholestatic and Genetic Diseases

JOURNAL OF HEPATOLOGY

Beta-amyloid deposition around hepatic bile ducts is a novel pathobiological and diagnostic feature of biliary atresia

Rosana Ottakandathil Babu[1,#], Vincent Chi Hang Lui[1,2,#], Yan Chen[3,#], Rachel Sze Wan Yiu[1], Yongqin Ye[4], Ben Niu[5], Zhongluan Wu[2], Ruizhong Zhang[3], Michelle On Na Yu[2,6], Patrick Ho Yu Chung[2,6], Kenneth Kak Yuen Wong[2,6], Huimin Xia[3], Michael Qi Zhang[5,7], Bin Wang[4,*], Urban Lendahl[1,8,*], Paul Kwong Hang Tam[1,2,6,*]

[1]*Dr. Li Dak-Sum Research Centre, The University of Hong Kong – Karolinska Institutet Collaboration in Regenerative Medicine, The University of Hong Kong, Hong Kong;* [2]*Department of Surgery, Li Ka Shing Faculty of Medicine, The University of Hong Kong, Hong Kong;* [3]*Department of Pediatric Surgery, Guangzhou Women and Children's Medical Center, Guangzhou Medical University, Guangzhou, China;* [4]*Department of General Surgery, Shenzhen Children's Hospital, Shenzhen, Guangdong, China;* [5]*Department of Biological Sciences, Center for Systems Biology, The University of Texas at Dallas, Dallas, Texas, United States of America;* [6]*Department of Surgery, University of Hong Kong-Shenzhen Hospital, Shenzhen, Guangdong, China;* [7]*MOE Key Laboratory of Bioinformatics, Center for Synthetic and Systems Biology, TNLIST, Tsinghua University, Beijing, China;* [8]*Department of Cell and Molecular Biology, Karolinska Institutet, Stockholm, Sweden*

Background and Aims: Biliary atresia (BA) is a poorly understood and devastating obstructive bile duct disease of newborns. It is often diagnosed late, is incurable and frequently requires liver transplantation. In this study, we aimed to investigate the underlying pathogenesis and molecular signatures associated with BA.

Methods: We combined organoid and transcriptomic analysis to gain new insights into BA pathobiology using patient samples and a mouse model of BA.

Results: Liver organoids derived from patients with BA and a rhesus rotavirus A-infected mouse model of BA, exhibited aberrant morphology and disturbed apical-basal organization. Transcriptomic analysis of BA organoids revealed a shift from cholangiocyte to hepatocyte transcriptional signatures and altered beta-amyloid-related gene expression. Beta-amyloid accumulation was observed around the bile ducts in BA livers and exposure to beta-amyloid induced the aberrant morphology in control organoids.

Conclusion: The novel observation that beta-amyloid accumulates around bile ducts in the livers of patients with BA has important pathobiological implications, as well as diagnostic potential.

Lay summary: Biliary atresia is a poorly understood and devastating obstructive bile duct disease of newborns. It is often diagnosed late, is incurable and frequently requires liver transplantation. Using human and mouse 'liver mini-organs in the dish', we unexpectedly identified beta-amyloid deposition – the main pathological feature of Alzheimer's disease and cerebral amyloid angiopathy – around bile ducts in livers from patients with biliary atresia. This finding reveals a novel pathogenic mechanism that could have important diagnostic and therapeutic implications.

Introduction

Biliary atresia (BA) is a devastating inflammatory cholangiopathy affecting 5–14:100,000 live births and is a predominant cause of prolonged neonatal jaundice.[1–3] BA affects the cholangiocytes of the liver both in the intrahepatic and extrahepatic biliary tree, leading to obstructed bile flow, progressive fibrosis and a subsequent breakdown of the bile duct system. As a first line treatment, patients with BA undergo Kasai portoenterostomy, in which bile duct tissue up to the porta hepatis is removed and a loop of jejunum is attached forming a portoenterostomy (for review see[4]). However, for many patients with BA, liver transplantation is the final outcome.

Diagnosis of BA is problematic. Missed or late diagnosis of BA leads to rapid liver deterioration, with liver transplantation the only remaining option. Hence, improvements in BA diagnosis are warranted (for review see[1,5]). However, poor understanding of the underlying pathogenic mechanisms of BA has led to slow progress in the field of diagnostics. Although BA affects >5:100,000 live births, it is not characterized by a strong genetic component: >90% of the cases are non-familial and without a clear genetic link (for review see[6]). Susceptibility loci have been identified on chromosomes 10q24.2[7] and 2q37.3,[8] and later, the *ADD3* and *EFEMP1* genes were identified as aberrantly regulated in BA.[9,10] Recently, mutations in the polycystic kidney disease 1 like 1 (*PKD1L1*) gene were also discovered in patients with BA splenic malformation syndrome, a form of BA with splenic abnormalities.[11] It is likely that BA has multiple etiologies, with

Keywords: Liver disease; Bile duct; Cholangiopathy; Organoid; Amyloid; Transplantation.
Received 24 July 2019; received in revised form 28 May 2020; accepted 4 June 2020; available online 16 June 2020

* Corresponding authors. Addresses: Department of General Surgery, Shenzhen Children's Hospital, Shenzhen, Guangdong, China. Tel.: +8613602576251; Fax: 0755-83008081. (B. Wang), or Department of Cell and Molecular Biology, Karolinska Institutet, Stockholm, Sweden. Tel.: +46-(0)8-524 873 23; Fax: +46-(0)8-468 308 37. (U. Lendahl), or Dr. Li Dak-Sum Research Centre, The University of Hong Kong – Karolinska Institutet Collaboration in Regenerative Medicine, The University of Hong Kong, Hong Kong. Tel.: +852-22554850; Fax: +852-28173155. (P.K.H. Tam).
E-mail addresses: szwb1967@126.com (B. Wang), urban.lendahl@ki.se (U. Lendahl), paultam@hku.hk (P.K.H. Tam).
[#] Co-first authors.
https://doi.org/10.1016/j.jhep.2020.06.012

viral infections, exposure to toxins and a dysfunctional immune response likely to contribute by causing inflammation and driving BA pathogenesis. Notably, mice infected by the rhesus rotavirus A (RRA) immediately after birth develop a BA-like phenotype,[12] and this model is widely used to study BA in an experimental *in vivo* setting.

In this report, we explore BA pathobiology through a combination of organoid and transcriptomic analyses. We find that liver organoids established from patients with BA, as well as from RRA-infected mice, exhibit aberrant morphology and apical-basal organization. Transcriptomic analysis revealed a partial shift from a cholangiocyte towards a hepatocyte transcriptional profile as well as changes in expression of genes related to beta-amyloid biology. We also observed beta-amyloid deposition close to bile ducts in patients with BA, which represents a novel pathobiological feature.

Materials and methods

Human liver tissues and liver organoid culture

Wedge liver biopsies (2–3 mm^3) were obtained from non-syndromic patients during laparoscopic cholangiography, and from pediatric patient controls (choledochal cysts [CC], cholestasis [CS] that were confirmed non-BA, non-tumor margin of hepatoblastoma [HB]). All tissues were obtained during operations with full informed consent from parents or patients, and the study was approved by Hong Kong West Cluster-Hong Kong University Cluster Research Ethics Committee/Institutional Review Board (UW 16-052).

Liver tissues were digested to single cells on gentleMACS™ Octo Dissociator (Miltenyi Biotec Inc. CA, USA), and EpCAM-positive cells were sorted on an MS column following the manufacturer's protocol (Miltenyi Biotec Inc. CA, USA). EpCAM-positive cells were then mixed with Matrigel (356231; Corning Biocoat) and seeded onto 4-well plates to generate organoids. See Supplementary Materials and Methods for details on the liver organoid generation, passaging and freezing.

Generation of RRA-infected mice

The RRA strain MMU 18006 was purchased from ATCC (Manassas, VA). The neonatal BALB/c mice were injected with 20 μl of 1.5×10^6 PFU/ml RRA (RRA group) or supernatant of MA104 cell culture medium (control group) intraperitoneally within 24 h of birth. Mouse liver organoids (RRA group and control group) were established using the same protocol as used for human liver organoids, except mouse CD326 (EpCAM) MicroBeads (130-105-958) were used to sort EpCAM-positive cells. All animal experiment protocols were approved by the Committee on the Use of Live Animals in Teaching & Research, The University of Hong Kong (CULATR No.: 4116-16).

Transcriptome sequencing and analysis

Organoids from controls and BA livers were retrieved from Matrigel to individual tubes (1 organoid per tube) for bulk RNA sequencing. See Supplementary Methods for details on the analysis of transcriptome sequencing data on the quality filtering of raw reads, transcriptome mapping/alignment with genome reference, counting of aligned reads per gene, normalization of gene expression count data, identification of differentially expressed genes and visualization.

10x sample processing, sequencing and analysis

Single cells from passage 0 (P0) organoids from 2 control patients (HB) were prepared. The processing of organoids for single-cell RNA sequencing analysis and the single-cell transcriptome data analysis were detailed as shown in the Supplementary Materials and Methods.

Treatment of human liver organoids with beta-amyloid

Beta-amyloid protein fragment 1-42 solution (AB9810, Sigma-Aldrich, St. Louis, USA; 1 mM in DMSO) was added to suspension of control (HB) organoid cells (final concentrations: 50 nM and 100 nM). The medium was changed with corresponding concentrations of beta-amyloid protein fragments (50 nM and 100 nM) and control (DMSO) every alternate day.

Immunostaining analysis

Liver tissues (HB, n = 5; CS, n = 3; CC, n = 34; BA, n = 46) or organoids in matrigel (from 4 HB non-tumor and 8 BA livers) were fixed in 4% paraformaldehyde (w/v) in PBS (pH 7.2) for 48 h at 4°C, dehydrated in graded series of alcohol, and cleared in xylene before being embedded in paraffin. Sections (6 μm in thickness) were prepared and mounted onto TESPA-coated microscope glass for immunostaining. Images were taken with a Nikon Eclipse E600 microscope mounted with a Nikon Digital Camera DXM1200F. Details of immunostaining procedures and antibodies are provided in the Supplementary Materials and Methods.

Protocols on histological analysis, RT-PCR analysis, quantitative RT-PCR analysis, transmission electron microscopic analysis, rhodamine transport assay, forskolin-induced swelling assay, TUNEL assay and measurement of organoid growth are reported in the Supplementary Materials and Methods.

Results

Liver organoids from patients with BA exhibit aberrant growth and morphology

Cells from the cholangiocyte lineage of mice and humans can be cultured in the form of three-dimensional organoids.[13–15] We used a stem cell type of organoid protocol[13] rather than a cholangiocyte-type protocol to more broadly explore whether organoids from patients with BA would differ from control organoids, for example with regard to differences in cholangiocytic *vs.* hepatocytic differentiation potential. Furthermore, this protocol has been successfully used to decode phenotypes from another cholangiopathy, Alagille syndrome (ALGS).[13,15] We established organoids from liver biopsies of 14 patients with BA at the time of Kasai, and as control organoids from liver biopsies of children with non-BA liver diseases including non-tumor liver of HB (n = 4); infantile CS (n = 4) and CC (n = 7) (organoid establishment, Fig. 1A; patient information, Fig. S1). Organoids grew from each patient type. In total 75 organoids were established from the 14 patients with BA, 19 organoids from the 4 patients with HB, 10 organoids from the 4 patients with CS, and 17 organoids from the 7 patients with CC.

Organoids from the patients with HB, CS and CC (referred to as “control” organoids) showed normal growth, whereas the majority of BA organoids exhibited aberrant growth and morphology (Fig. 1B,C). Small organoids appeared from controls in 3–5 days, and grew into large, well-expanded cystic structures with a single outer layer of epithelial cells in 20 to 30 days (Fig. 1B). Control organoids were passaged for sub-culturing when they grew beyond the size limit (between 20 to 30 days)

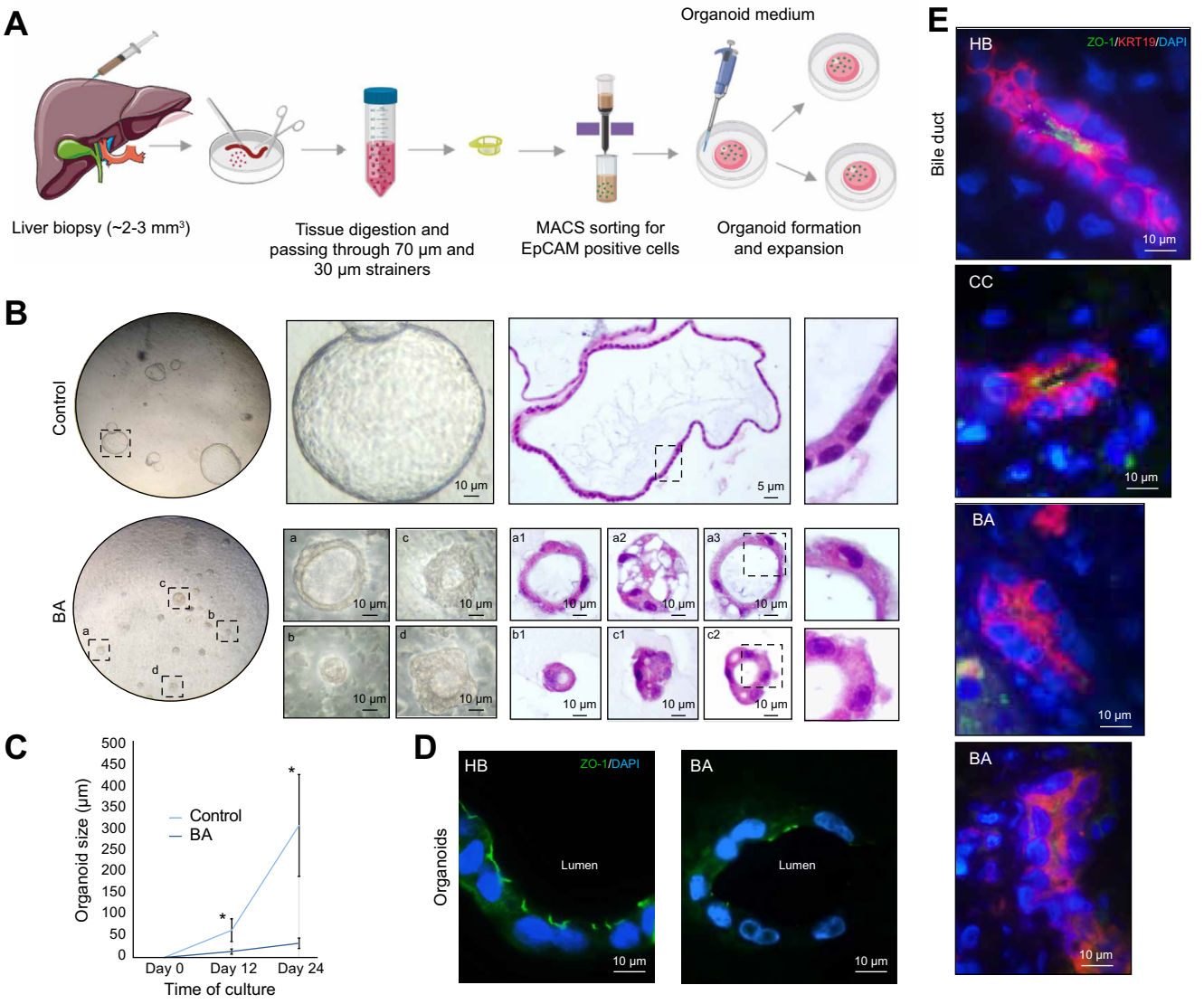

Fig. 1. Liver organoids from patients with BA exhibit aberrant morphology. (A) Schematic diagram of liver organoid establishment from liver biopsies. (B) Representative bright field images of the organoid cultures from liver biopsies of a patient with HB (control) (upper set) and a patient with BA (lower set). Marked and highlighted organoids (broken lined squares) are shown at high magnification to the right. Histological sections of the control organoid, the BA organoids "a, b, c and d" (a1–a3, c1–2 were consecutive sections of organoids "a" and "c", respectively) are shown. The epithelial cell layers (highlighted) of the control and BA organoids are shown at high magnification to the right. (C) Growth curve (organoid size) of P0 (passage zero) primary organoids of control (HB, n = 4; CC, n = 2) and BA (n = 6) patients (*p <0.05, Student's t test). (D) ZO-1 staining of control and BA organoids. P0 primary organoids of HB (n = 4) and BA (n = 8) were included for the morphological, histological and ZO-1 immunostaining. (E) Representative images of ZO-1 and KRT19 co-staining of bile ducts of patients with HB (n = 2), CC (n = 2) and BA (n = 6). BA, biliary atresia; CC, choledochal cyst; CS, cholestasis; HB, hepatoblastoma. (This figure appears in color on the web.)

and could be maintained in culture for more than 6 months, frozen and re-established after freezing. Control organoids expanded at the pace expected for healthy organoids[13] and developed a spherical shape with a cuboidal single-cell layer of epithelial cells and a single vacuole inside (Fig. 1B). BA organoids, in contrast, while appearing in 3–5 days, were irregular in shape and loosely packed and grew less well, frequently appearing either as poorly expanded structures with multiple vacuoles and a thick cell layer ("multi-vacuole organoids") (Fig. 1B(a) and 1B(a1–a3)) or as unexpanded cell clusters with an irregular multicellular outer cell layer ("unexpanded organoids") (Fig. 1B(b–d) and 1B(b1–c2)). 50–85% of the BA organoids fell into the "unexpanded" category and 15–50% of the BA organoids belonged to the "multi-vacuole" category, while all of the control organoids qualified as normal (Fig. 1B). Due to their slow growth (Fig. 1C), no passage was needed after 90 days in culture for BA organoids; in fact, BA organoids, in contrast to control organoids, could not be dissociated into single cells for sub-culturing and could not be passaged. To explore the growth differences further, we performed immunostaining for Ki67 and the TUNEL assay to assess proliferation and cell death, respectively. The percentage of Ki67 immuno-positive proliferative cells in BA organoids was significantly lower than in control organoids (mean ± SEM: 15.9 ± 2.1 *vs.* 28.6 ± 2.4; p <0.05) (Fig. S2A). However, no significant difference in cell death was observed, as determined by TUNEL staining (Fig. S2A; Fig. S2B).

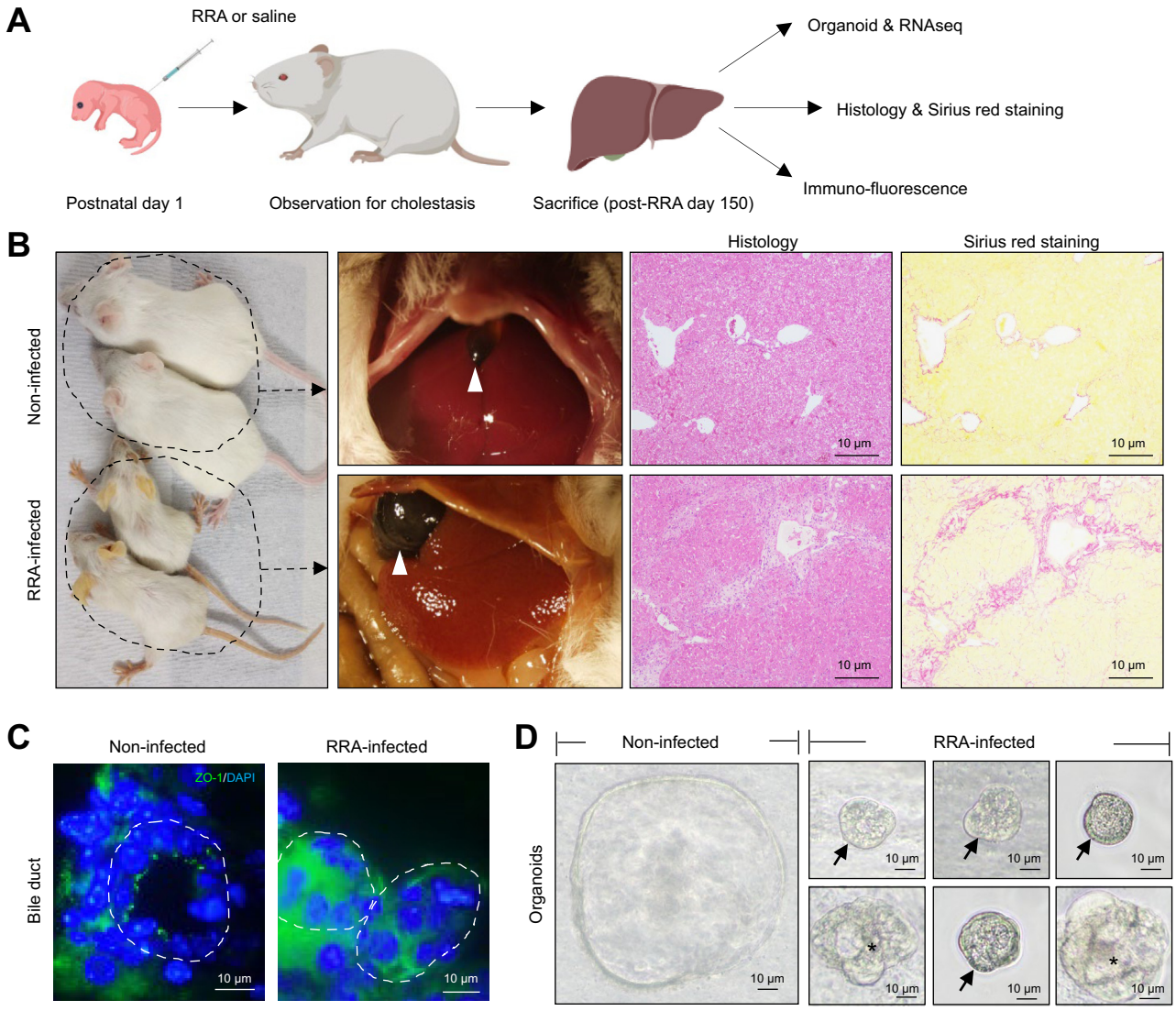

Fig. 2. Organoids from RRA-infected mice show BA-like morphological aberrations. (A) Schematic depiction of RRA infection and subsequent analysis. (B) At post-RRA day 150, RRA-infected mice were smaller and showed signs of jaundice (yellowish) at the ears, paws and tails. The gallbladder (arrowhead) was enlarged, histology and Sirius Red staining of RRA-infected mouse livers (n = 4) revealed fibrosis at the portal areas and inter-lobular regions. None of these BA features were detected in non-infected mice (n = 3). (C) Representative photos of ZO-1 staining of the liver sections of non-infected control (n = 3) and RRA-infected mice (n = 4) at post-RRA day 150. (D) Representative bright field photos of P0 primary organoids from the non-infected control liver (n = 3) and the RRA-infected mice (n = 4). RRA organoids were generally smaller, and either with multiple vacuoles (*) or with a multicellular outer layer (arrows). RRA, rhesus rotavirus A. (This figure appears in color on the web.)

The aberrant morphology of the BA organoids may indicate problems in cell polarity, and to assess this, we first analyzed the distribution of Zona occludens 1 (ZO-1), a marker for tight junctions at apical intercellular junctions. In control organoids, ZO-1 formed a smooth layer at the apical side of the cells as expected, while the ZO-1 distribution was scattered in the BA organoids, without a clear apical predominance (Fig. 1D). A scattered ZO-1 distribution without clear apical predominance was also evident in the biliary epithelia of patients with BA (n = 6), while biliary epithelia from control livers (HB and CC) showed a predominantly apical ZO-1 immunoreactivity (Fig. 1E). Furthermore, cystic fibrosis transmembrane conductance regulator (CFTR) immunohistochemistry revealed that the polarized expression of CFTR at the luminal side in control organoids was strongly reduced in BA organoids, which had a lower level and more even distribution of CFTR in the cells (Fig. S2C1). Similarly, the expression of secretin receptor (SCTR) at the extraluminal surface in control organoids was replaced with a more diffuse distribution in the BA organoids (Fig. S2D). The polarized expression of gamma glutamyltransferase (GGT) and solute carrier family 10 member 2 (SLC10A2, aka ASBT) at the intraluminal side in control organoids was also largely absent in the BA organoids (Fig. S2E; Fig. S2F).

To functionally assess cell polarity, we tested the activity of CFTR, using the Forskolin swelling assay.[16] Control organoids underwent swelling by 11 ± 0.02% (Mean ± SD) following 30 min of Forskolin stimulation, while Forskolin failed to induce BA organoid swelling (Fig. S3A), indicating that CFTR activity was

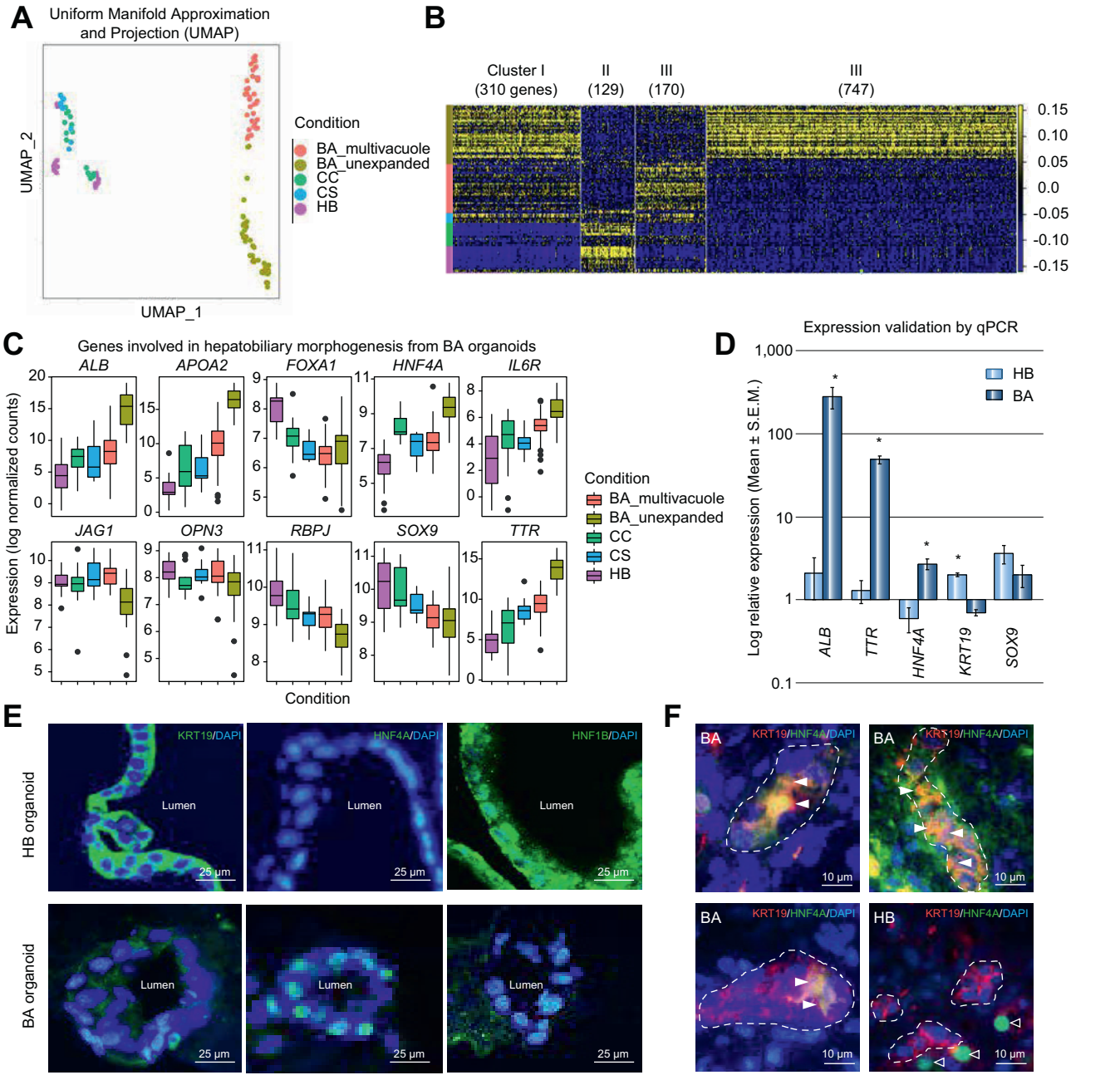

Fig. 3. Transcriptomic analysis and defective hepatobiliary differentiation in BA. (A) UMAP showing clustering of n = 121 bulk transcriptomes from organoid samples from BA and controls (CC, SC, HB); each dot represents an organoid. (B) Heatmap showing the mRNA expression levels of total DEGs (n = 1,356) in BA categories when compared to controls (yellow – high expression; blue – low/no expression). Each column represents a gene and each row represents an organoid from the conditions indicated by color bars to the right. For a complete gene list, see Table S4 online. (C) Boxplot showing the expression patterns of topmost hepatobiliary genes that are differentially regulated in BA at $p < 0.05$ (2-tailed Student's *t* test). The dots represent the suspected outlier sample data points (each dot is an organoid sample) which is objective in normally distributed expression dataset. (D) Expression validation by qPCR for *ALB, TTR, HFN4A, KRT19* and *SOX9* mRNA expression in the primary organoids. Normalized expressions of *ALB, TTR, HFN4A, KRT19* and *SOX9* between control *vs.* BA organoids were compared (*$p < 0.05$, Student's *t* test; P0 primary organoids of 4 HB *vs.* P0 primary organoids of 4 BA). (E) Representative photos of sections of control (HB; n = 4) and BA (n = 8) P0 primary organoids stained for cholangiocyte (KRT19, HNF1B) and hepatocyte (HNF4A) markers. (F) Representative images of KRT19 and HNF4A co-staining on BA and HB livers showing KRT19/HNF4A double-positive cells (filled arrowheads) in BA livers (n = 6), but not in HB livers (n = 4). Unfilled arrowheads indicate HNF4A single-positive hepatocytes in HB livers. Broken lines indicate bile ducts. BA, biliary atresia; CC, choledochal cyst; CS, cholestasis; DEG, differentially expressed gene; HB, hepatoblastoma; UMAP, uniform manifold approximation and projection. (This figure appears in color on the web.)

abrogated in BA organoids. In an attempt to test the activity of multidrug resistance protein 1 (MDR1), which encodes a transmembrane export pump in cholangiocytes[17] and pumps compounds into the lumen of organoids,[18] we added the MDR1 fluorescent substrate Rhodamine 123 (R 123) to the culture medium. In the presence of verapamil, which blocks MDR1

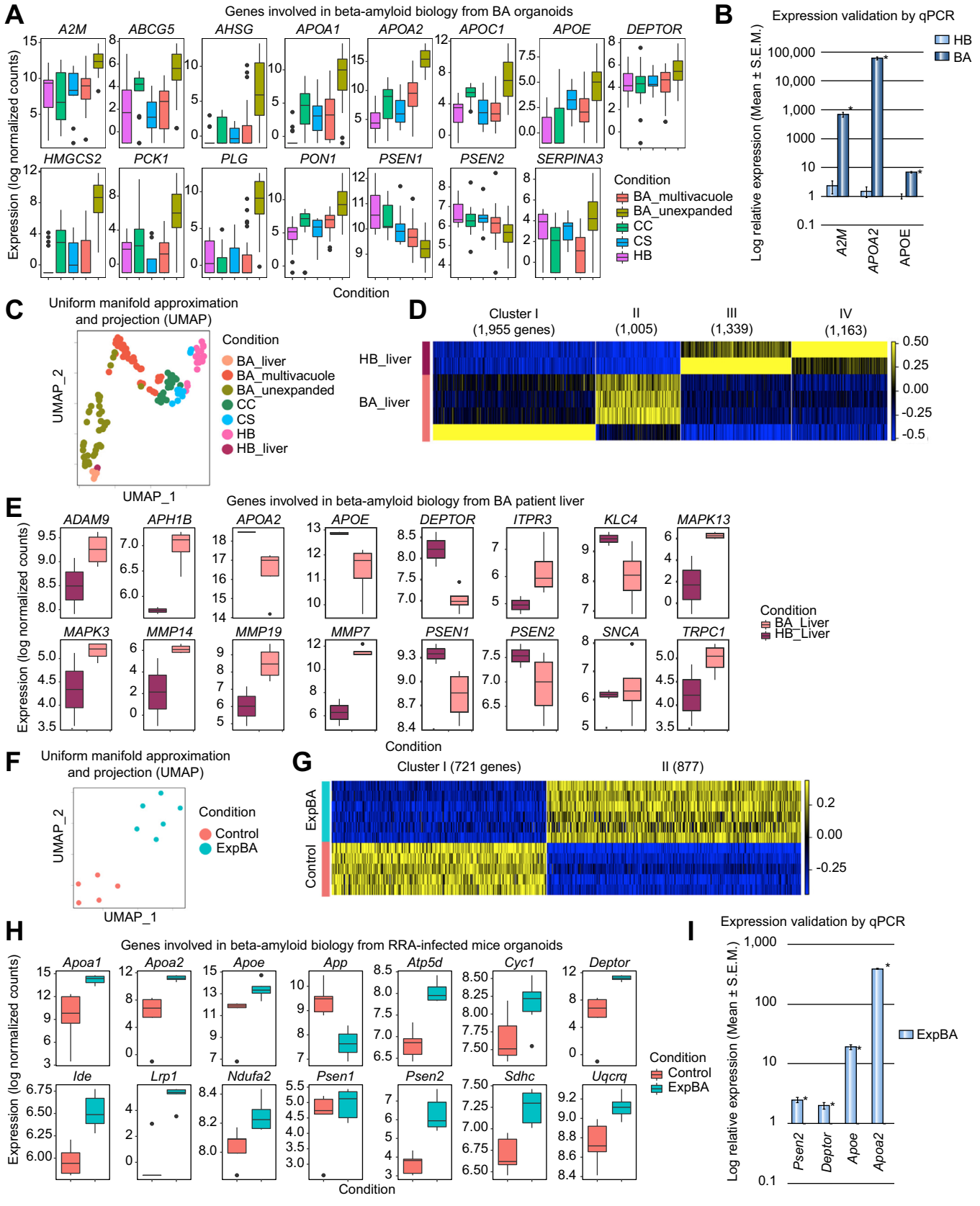

Fig. 4. Expression profiles of genes involved in beta-amyloid biology. (A) Boxplot showing the mRNA expression levels of topmost beta-amyloid pathway-related genes in BA *vs.* control organoids at $p < 0.05$ (2-tailed Student's *t* test). (B) Expression validation by qPCR for *A2M*, *APOA2* and *APOE*. Normalized expressions of *A2M*, *APOA2* and *APOE* between control (HB; n = 4) *vs.* BA (n = 4) organoids were compared (*$p < 0.05$, Student's *t* test). (C) UMAP projection showing the bulk transcriptome expression

activity, as expected, there was no accumulation of R 123 in the control organoids (Fig. S3B). In contrast, R 123 accumulated in the lumen of BA organoids in the presence of verapamil, which may be a result of dysfunctional tight junction organization in the BA organoids.

We then used transmission electron microscopy (TEM) to gain further insights into cellular organization. TEM analysis showed normal basal-apical polarity in control organoids, as demonstrated by the presence of pinocytic vesicles, monolayer of cells with tight junctions, lateral inter digitation, apical microvilli, and primary cilia; all typical characteristics of biliary epithelial cells[19] (Fig. S4A–F). In contrast, tight junctions were not observed in BA organoids (Fig. S5A). To corroborate these findings, we conducted TEM on histological sections from bile ducts of patients with BA and HB. Similar to the situation in the organoids, tight junctions were observed in the bile ducts of HB but not of BA livers (Fig. S5B). In sum, these data reveal specific changes in morphology and apical-basal organization in organoids from patients with BA.

Organoids from RRA-infected mice show morphological aberrations similar to those observed in patients with BA

We were next interested in exploring whether morphological alterations could be observed in organoids from RRA-infected mice, a well-established experimental BA model.[12] RRA inoculation of mice (Fig. 2A) produced the expected symptoms (smaller body size, jaundice, extrahepatic bile duct atresia, enlarged gallbladder and fibrosis at the portal areas and interlobular regions of the livers) (Fig. 2B). ZO-1 immunohistochemistry showed a scattered ZO-1 distribution without a clear apical predominance in the RRA-infected biliary epithelia, in contrast to the predominantly apical ZO-1 immunoreactivity in the non-infected control liver (Fig. 2C). Organoids from the RRA-infected mice (referred to as RRA organoids) were established 150 days after viral infection and exhibited aberrant morphology, similar to that observed in organoids from patients with BA. Specifically, RRA organoids showed slow growth and produced spheres with multiple vacuoles or a multicellular outer layer, or alternatively appeared as unexpanded cell clusters of irregular shape (Fig. 2D). In contrast, organoids from non-infected mice showed the growth characteristics expected for wild-type mouse organoids[14] (Fig. 2D). Together, these data show that organoids from RRA-infected mice exhibit an aberrant morphology similar to that observed in organoids from patients with BA.

Organoids from patients with BA transcriptomically shift from a cholangiocytic towards a hepatocytic fate

We subjected 121 organoids from patients with BA and controls (HB, CS and CC) to bulk transcriptome analysis[20] (analysis pipeline and quality control, Fig. S6A–C). Uniform manifold approximation and projection (UMAP) analysis revealed that the "multi-vacuole" and "unexpanded" organoid transcriptomes appeared as 2 separate clusters although with some internal heterogeneity, which may reflect the different morphologies and sizes of BA organoids. The 2 BA clusters were well-separated from the HB, CS and CC organoid clusters (Fig. 3A; principal component analysis [PCA] Fig. S7A). There was also some heterogeneity in the control clusters, probably related to differences in age and disease severity.

A heatmap of 1,356 differentially expressed genes (DEGs) between BA and control organoids revealed 4 groups of genes that differed between the control (HB, CS and CC) and BA organoids. The transcriptomic profiles for the "unexpanded" and "multi-vacuole" BA organoid transcriptomes were quite distinct (Fig. 3B). The "unexpanded" transcriptomes showed the largest gene expression differences compared to the controls, while the "multi-vacuole" transcriptomes were closer to the control transcriptomes and in particular to the CS transcriptomes (Fig. 3B). The HB, CS and CC transcriptomes exhibited less but distinct transcriptomic differences, with some outlier organoids, particularly in the HB and CC controls. The most high-ranking gene ontology (GO) categories and pathways for BA organoids (Fig. S7B–D) include lysosome organization, bile acid metabolic process and regulation of cell proliferation.

Both cholangiocytes and hepatocytes originate from hepatoblast progenitors,[21] and we observed expression of the adult stem cell markers LGR5 and PROM1 in organoids (Fig. S8A). We next assessed whether genes involved in hepatobiliary differentiation[22,23] were differentially expressed. Control organoids expressed markers for liver progenitors (*AFT*, *EPCAM*, *LGR5*, *PROM1*), bile duct cell fate (*CFTR*, *KRT7*, *KRT19*, *SOX9*) and the hepatocyte lineage (*HNF4A*, *TBX3*) (Fig. S8A). Single-cell RNA sequencing of control liver (HB) organoids revealed that approximately 88% and 12% of the cells were classified as cholangiocytes and hepatoblasts, respectively (Fig. S8B,C). Furthermore, the *TACSTD2* gene, which encodes the TROP2 protein that was recently shown to be a marker for cells that can give rise to bipotent organoids,[24] was expressed both in control (HB; CC; CS) and BA organoids (Fig. S8D), suggesting that both control and BA organoids were derived from a common progenitor cell type. The BA organoids showed altered expression of a number of hepatobiliary genes. Several genes involved in cholangiocyte development were downregulated in BA organoids, including *FOXA1, JAG1, OPN3, RBPJ and SOX9*, while genes involved in hepatocyte development, including *ALB, APOA2*, *HNF4A*, *IL6R and, TTR*, were upregulated (Fig. 3C; additional gene examples, Fig. S8E). Significant downregulation of *KRT19* and upregulation of *ALB*, *HNF4A* and *TTR* mRNA expression was demonstrated by qPCR (Fig. 3D). There was a trend towards downregulation of *SOX9*, but this did not reach statistical significance. To corroborate

profiles of 121 organoids (from Fig. 3A) along with the bulk transcriptome from liver tissues of 2 patients with HB (second HB_liver sample is overlapping with the first one) and 4 with BA (labelled as HB_Liver and BA_Liver, respectively); each dot represent organoids and liver samples. For a complete gene list, see Table S4 online. (D) Heatmap showing the mRNA expression levels of total genes (n = 5,462) that are differentially expressed in BA livers compared to HB control. (E) Boxplot showing the mRNA expression levels of topmost beta-amyloid pathway-related genes in BA and control livers at p <0.05 (2-tailed Student's t test). (F) UMAP plot showing the bulk transcriptome expression profiles of organoids from RRA-infected (ExpBA) and non-infected mice (Control); each dot represents 1 organoid. For a complete gene list, see Table S4. (G) Heatmap showing the mRNA expression levels of total DEGs (n = 1,598) in mouse RRA experimental BA organoids when compared to control. (H) Boxplot showing the mRNA expression levels of topmost beta-amyloid pathway-related genes in RRA-infected *vs.* non-infected mouse livers at p <0.05 (2-tailed Student's t test). (I) Expression validation by qPCR for beta-amyloid genes in mouse organoids (P0 primary organoids form 2 control mouse livers and 4 BA mouse livers). Logarithmic values of the relative expression of genes between BA and normal mouse organoids are shown. The relative expression of genes in normal organoids were arbitrarily regarded as 1.0 (*p <0.05, Student's t test). BA, biliary atresia; DEG, differentially expressed gene; HB, hepatoblastoma; RRA, rhesus rotavirus A; UMAP, uniform manifold approximation and projection. (This figure appears in color on the web.)

expression differences at the protein level, immunostaining for KRT19 and HNF1B protein was reduced, while HFN4A immunoreactivity was elevated in BA organoids (Fig. 3E). The presence of HNF4A/KRT19 double-positive bile duct cells was only detected in BA livers (n = 6), but not in control HB livers (n = 4) (Fig. 3F). In sum, BA organoids display a shift towards a hepatocytic gene expression profile.

Organoids from patients with BA and RRA-infected mice show beta-amyloid-associated transcriptional signatures

The GO and pathway analysis revealed DEGs involved in Alzheimer's disease (AD) secretase (P00003) and AD-presenilin (P00004) pathways to be differentially expressed in the BA organoids (Fig. S7C,D). To further address a potential link to beta-amyloid biology, supervised marker analysis was carried out using marker genes from amyloid-related AD pathways (P00003, P00004 and hsa05010) and from the literature[22,25–30] (for review see[31]), and a total of 111 such genes were differentially regulated in BA organoids (Fig. S9). DEGs include *A2M*, *APOA1*, *APOA2*, *APOE*, *DEPTOR*, *HMGCS2*, *PSEN1* and *PSEN2* (Fig. 4A; additional genes, Fig. S9). The differential expression of *A2M*, *APOA2* and *APOE* was further validated by qPCR (Fig. 4B).

To corroborate these findings, we next analyzed gene expression changes in bulk transcriptomes from liver biopsies of 4 patients with BA and 2 with HB. The 4 BA patient transcriptomes clustered distinctly from the 2 HB patient transcriptomes but closer to BA "unexpanded" in a UMAP analysis (Fig. 4C; PCA analysis, Fig. S10A). A heatmap of 5,462 DEGs between BA and control livers (*p* value cut-off ≤0.05) corroborated the differences between BA and HB transcriptomes, although 1 BA liver transcriptome clearly represents an outlier (Fig. 4D), for reasons that are not understood. A number of genes associated with beta-amyloid biology were differentially regulated in the BA livers, including *ADAM9*, *APOE*, *DEPTOR*, *ITPR3*, *MMP7*, *PSEN1* and *PSEN2* (Fig. 4E; complete list of differentially expressed beta-amyloid biology genes, Fig. S10B). Notably, matrix metalloprotease 7 (*MMP7*), which has recently been identified as a marker for BA, was the most differentially expressed.[32] The most high-ranking GO categories and pathways (Fig. S10C,D) include actin cytoskeleton organization, integrin-mediated signaling and angiogenesis pathways.

To further assess a potential link to deregulated beta-amyloid processing, we analyzed bulk transcriptomes of organoids from control and RRA-infected mice. The transcriptomes from 5 control organoids (from non-infected mice) and 6 RRA organoids formed distinct clusters in a UMAP analysis (Fig. 4F; PCA analysis, Fig. S11A). Differential gene expression analysis revealed 1,598 DEGs (*p*-value cut-off ≤0.05) and underscored the heatmap clustering of the control and RRA organoids (Fig. 4G). Several genes associated with beta-amyloid biology were differentially regulated, including *App*, *Apoa2*, *Apoe*, *Deptor*, *Lrp1*, *Psen1*, *Psen2* and *Sdhc*; (Fig. 4H; Fig. S11B). qPCR analysis validated the upregulation of *Apoa2*, *Apoe*, *Deptor* and *Psen2* in RRA organoids (Fig. 4I). The most high-ranking GO categories and pathways (Fig. S11C,D) include response to virus, blood coagulation and lipid metabolic process.

The transcriptomic data from the human liver and RRA organoids also reveal changes in expression of hepatobiliary genes, in keeping with the results presented for BA organoids in Fig. 3A. Thus, *KRT8* showed increased expression in BA livers, while *OPN3*, *HNF1B*, *HHEX*, *FOXA1*, *FOXA2* and *HES1* were downregulated (Fig. S12A). Similarly, in the mouse RRA organoids, *Sox9*, *Jag1*, *Hhex*, and *Hnf1b* were downregulated while the hepatocyte markers *Hnf4a*, *Apoa2*, and *Ttr* were upregulated (Fig. S12B; qPCR validation, Fig. S12C). In conclusion, the transcriptomic data indicate that beta-amyloid metabolism may be altered in BA.

Accumulation of beta-amyloid deposits around bile ducts in livers from patients with BA and RRA-infected mice as well as around BA organoids

The data described previously indicate that APP processing or metabolism may be altered in BA. The beta-amyloid peptide (Aβ peptide) is generated by β- and γ-secretase processing of APP; the Aβ peptide is the main constituent in beta-amyloid, which accumulates as plaques in diseases such as AD and cerebral amyloid angiopathy (CAA).[33] To learn whether beta-amyloid deposits are present in livers from patients with BA, beta-amyloid immunoreactivity was analyzed (using an antibody recognizing amino acid residues 17-24 of APP) in histological sections from BA livers (n = 46) and livers of HB (n = 5), CS (n = 3) and CC (n = 34) as control. Beta-amyloid deposits were specifically found in the BA livers, where they localized within the biliary epithelial cells or in the bile duct lumen (Fig. 5A, Fig. S13). Occasionally, amyloid deposits were detected at non-bile duct liver cells in close proximity to the bile ducts (Fig. 5A). On average, 87% ± 18% of bile ducts in BA livers were beta-amyloid immunopositive, while no immunoreactivity was observed in the controls.

In RRA-infected mice, beta-amyloid deposits were found in biliary epithelial cells as well as in non-bile duct liver cells in close proximity to bile ducts (Fig. 5B). No beta-amyloid immunoreactivity was detected in the bile ducts of non-infected control livers (Fig. 5B). Finally, we show that beta-amyloid was observed around BA but not HB organoids (Fig. 5C). In conclusion, beta-amyloid accumulates around bile ducts in livers of patients with BA and RRA-infected mice, as well as around BA organoids.

Exogenous beta-amyloid induces BA-related morphological and transcriptional changes in liver organoids

To test whether beta-amyloid alone was sufficient to replicate morphological and transcriptional changes in organoids, we treated organoids from human control livers with Aβ peptide 1–42 for 7 days or with DMSO alone as untreated control. Control organoids exposed to beta-amyloid were generally very small and appeared as poorly expanded spheres with small vacuoles or with multiple vacuoles surrounded by a monolayer of cells (Fig. 6A).

Bulk transcriptomes from beta-amyloid-treated control organoids clustered close to "multi-vacuole" BA patient organoid transcriptomes (organoid data are derived from Fig. 3A), while untreated organoids showed a normal morphology (Fig. 6A) and transcriptomically localized further away from the BA transcriptomic clusters and near the control (HB) transcriptome clusters (Fig. 6B; PCA analysis, Fig. S14A). Differential gene expression analysis revealed 6,495 DEGs (*p*-value cut-off ≤0.05) and corroborated the UMAP clustering (Fig. 6C; for GO analysis see Fig. S14B,C), although there was some divergence among the beta-amyloid-treated organoids. *SOX9* and *HHEX* were among the downregulated genes, while *HNF4A*, *KRT18*, and *KRT8* were among the upregulated genes in organoids upon beta-amyloid exposure (Fig. 6D), indicating a shift towards a

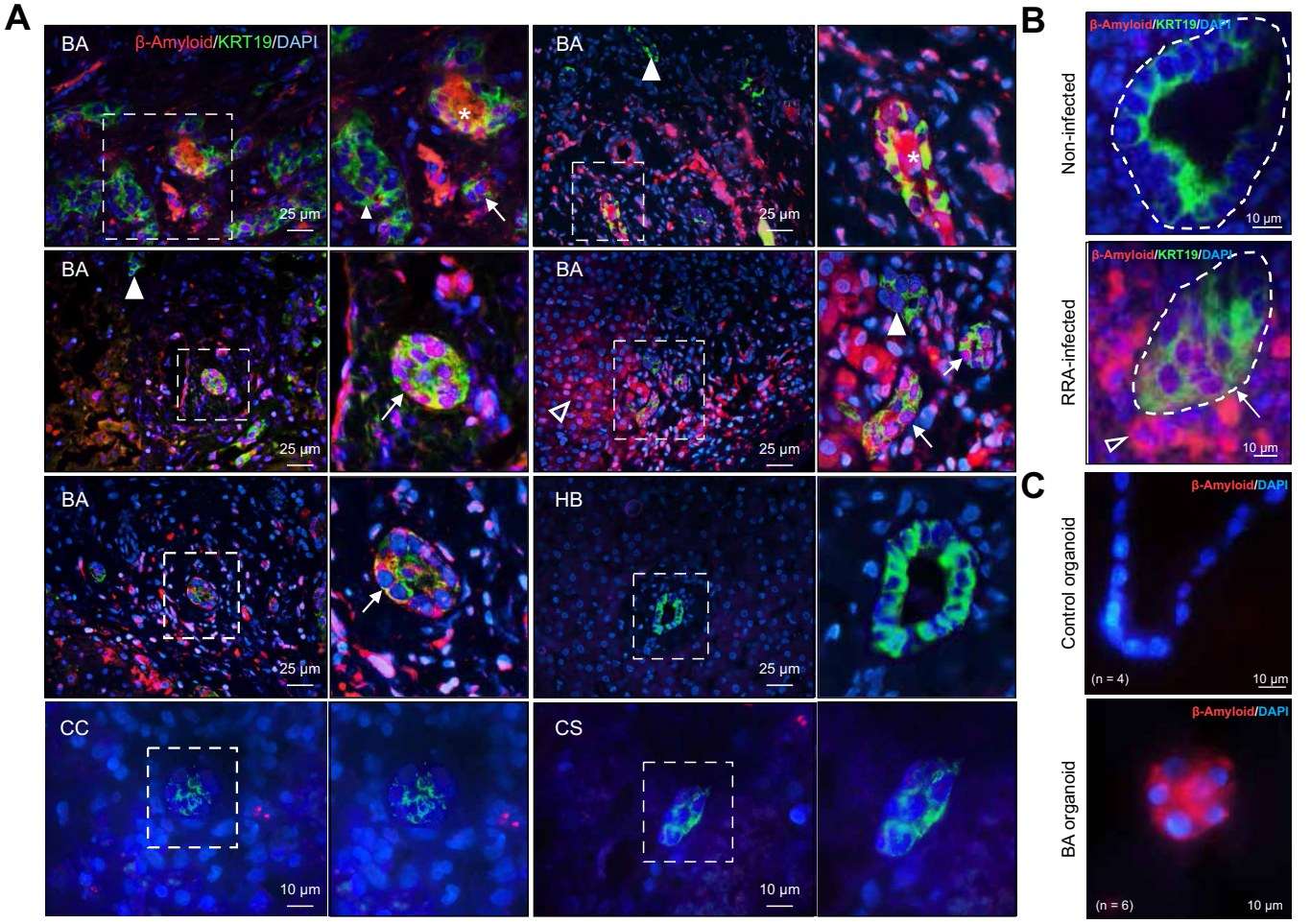

Fig. 5. Immunohistochemistry staining for beta-amyloid in human and mouse liver tissues, and in human organoids. (A) Representative images of co-staining of liver tissue sections from BA and control (HB; CC; CS) patients with beta-amyloid (red) and KRT19 (green) antibodies. (B) Representative images of co-staining of liver tissue sections from RRA-infected (n = 4) and non-infected control mouse (n = 3) livers with beta-amyloid (red) and KRT19 (green). (C) Representative images of staining of organoids from control (HB; n = 4) and BA (n = 6) with beta-amyloid (red). DAPI staining is shown in blue. BA, biliary atresia; CC, choledochal cyst; CS, cholestasis; DEG, differentially expressed gene; HB, hepatoblastoma; RRA, rhesus rotavirus A. (This figure appears in color on the web.)

hepatocytic fate. A number of genes involved in beta-amyloid biology were differentially regulated in the beta-amyloid-treated control organoids (Fig. 6E). Cross-comparison of the DEGs involved in beta-amyloid biology between beta-amyloid-treated control organoids and patient-derived BA organoids (136 and 111 genes from Fig. S9 and Fig. S15, respectively) revealed 16 genes that were differentially expressed in both settings (Fig. 6F). In sum, the data show that exposure of control organoids to beta-amyloid induces morphological and transcriptomic changes reminiscent of those observed in BA organoids.

Discussion

BA is a severe liver disease in which bile flow obstruction leads to progressive fibrosis. Liver transplantation is the final outcome if Kasai portoenterostomy does not alleviate the problems. Meanwhile, the diagnosis of BA has remained problematic; improved diagnosis is important for stratifying patients and guiding treatment decisions.

In this report, we use a combination of transcriptomics and organoid biology to gain new insights into the molecular underpinnings of BA. Unexpectedly, beta-amyloid deposition was observed around the bile ducts of both patients with BA and in RRA-infected mice. BA thus joins the ranks of diseases characterized by beta-amyloid aggregation; a list comprising AD and CAA, but also inclusion body myositis[34] and dementia with Lewy bodies (for review see[35]). The link between beta-amyloid deposition and BA is corroborated by transcriptional analysis of BA patient liver biopsies and liver organoids, as well as of RRA-infected mouse livers, which show altered expression of several genes involved in APP processing and the AD-secretase pathway. Liver organoids from patients with BA or RRA-infected mice displayed an aberrant morphology, and similar aberrations could be induced in human control organoids by exposing them to exogenous beta-amyloid. The latter finding may indicate that beta-amyloid accumulation contributes to bile duct pathology in BA, but more research is required to address whether beta-amyloid deposits are a cause, a cell-stress mediator, or a bystander effect, resulting from other upstream dysregulated processes.

The beta-amyloid deposits were found specifically in liver biopsies from patients with BA, and not in livers from patients

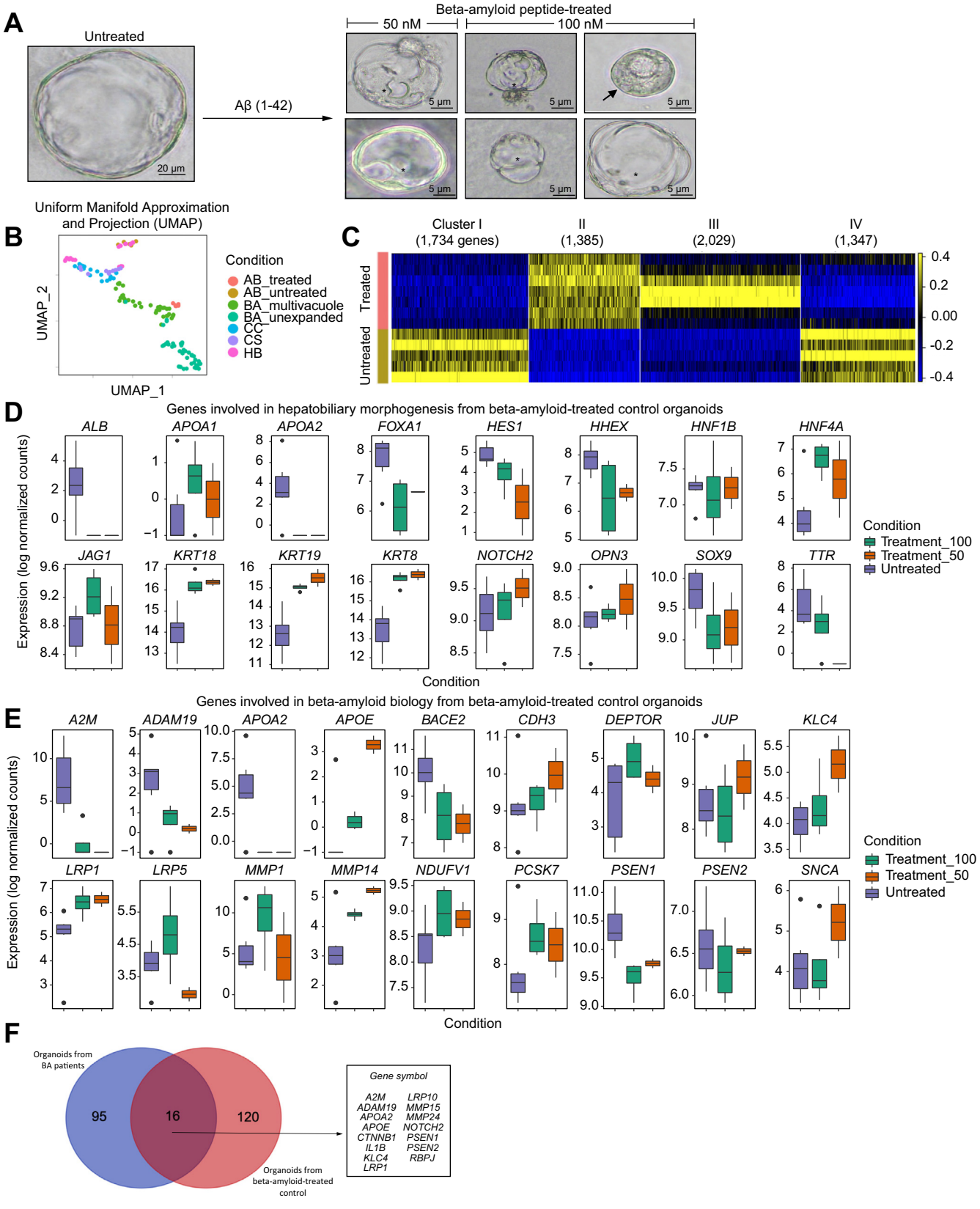

Fig. 6. Beta-amyloid-treated control organoids show BA-like morphological aberrations and transcriptomic profiles. (A) Organoid morphology of beta-amyloid-treated (50 nM and 100 nM) and untreated P1 control organoids. (B) UMAP showing bulk transcriptome expression profile of 121 organoids from patients with BA and controls (from Fig. 3A) along with transcriptomes from beta-amyloid-treated and untreated control organoids; each dot represents an

with HB, CS or CC, and could thus be considered as a new diagnostic feature for BA. The need for improved diagnosis is underscored by the fact that outcomes are improved when surgery is performed at an early age[36–38] (for review see[5]). Advances in BA diagnosis, including altered expression of specific miRNAs (miR-140-3p; miR-200b/429 and MiR-4429)[39–41] and elevated serum levels of MMP7 have been shown to be highly prognostic for BA.[32,42] While MMP7 analysis can be carried out on blood samples, we do not yet know whether this is feasible for beta-amyloid. However, we believe that analysis of beta-amyloid may have the potential to become a complementary assay to further optimize diagnosis. Sensitive assays to monitor minute quantities of beta-amyloid have been developed in AD research (for review see[43]) and these assay systems may be used to derive information from extremely small biopsies of patients with putative BA in the future; needle biopsies, although invasive, are frequently carried out for routine pathology. It is interesting to note that *MMP7* was the most highly upregulated gene from the DEGs in our transcriptomic analysis from BA livers, which indicates that the high MMP7 serum levels[32,42] are a result of increased mRNA expression of the *MMP7* gene.

The organoids from both patients with BA and RRA-infected mice grew more slowly and displayed an aberrant morphology, characterized by poor expansion with multiple vacuoles and a thick, frequently multicellular outer cell layer. We observed 2 distinct morphologies, “multi-vacuole” and “unexpanded”, and the distinction between these 2 types was also manifested at the transcriptome level, where the “unexpanded” transcriptomes were the most distantly related to the controls. The aberrant organoid morphology appears specific for BA, *i.e.* it was only observed in BA organoids, and not in organoids from patients with HB, CS or CC. Liver organoids have previously been used to model pathogenesis in the dish for liver diseases with a clear-cut monogenic basis, such as α1-antitrypsin-deficiency and ALGS.[13,15] Our data show that they can also be used to study a liver disease with more complex etiology, and with only a few characterized susceptibility genes, such as *ADD3*, *EFEMP1* and *PKD1L1*.[9,11] It will be interesting to explore whether an organoid phenotype can be induced by other agents that have been implicated in BA pathogenesis, for example viral and bacterial infections, toxins, and inflammation.[1,5] Notably, the BA-inducing effects of biliatresone in animal models have recently been recapitulated using cholangiocyte mouse organoids, and these studies also reveal cell polarity problems in the biliatresone-treated organoids.[44,45] Conversely, it will be important to address whether the observed morphological aberrations can be revoked, which would make the BA organoids excellent tools as a drug-screening platform for novel BA therapeutic approaches.

The aberrant morphology in BA organoids was accompanied by dysregulated apical-basal polarity in the cells of the outer layer of the organoid as well as in BA livers, as determined by altered localization of apical-basal markers such as ZO-1, CFTR, SCTR, GGT and ASBT. Disturbed ZO-1 distribution, coupled with dysregulated expression of several apical-basal genes, was also noted in patients suffering from ALGS.[15] This raises a more general question of possible similarities, notably with regard to apical-basal polarity, between ALGS and BA, 2 cholangiopathies with similarities in pathology. The transcriptomic analysis of the BA liver organoids indicates that the cholangiocyte phenotype may be partially shifted towards a hepatocytic fate, and the biliary marker *SOX9* expression is also downregulated in ALGS,[15,46] further supporting a possible mechanistic link between these 2 cholangiopathies.

In conclusion, our data reveal aberrant morphology and apical-basal organization in BA organoids, as well as a partial shift from a cholangiocyte towards a hepatocyte transcriptional profile and changes in expression of genes related to beta-amyloid biology. We also present a new pathobiological feature of BA – beta-amyloid deposition around bile ducts in BA livers. While our data indicate that beta-amyloid can induce the observed morphological changes in organoids, more work is required to understand whether beta-amyloid accumulation is causative in the disease process or a bystander effect resulting from other disease-causing mechanisms, for example problems in apical-basal organization.

Abbreviations

AD, Alzheimer's disease; ALGS, Alagille syndrome; BA, biliary atresia; CAA, cerebral amyloid angiopathy; CC, choledochal cyst; CFTR, cystic fibrosis transmembrane conductance regulator; CS, cholestasis; DEG(s), differentially expressed gene(s); GGT, gamma glutamyltransferase; GO, gene ontology; HB, hepatoblastoma; MMP7, matrix metalloprotease 7; PCA, principal component analysis; RRA, rhesus rotavirus A; SCTR, secretin receptor; TEM, transmission electron microscopy; UMAP, uniform manifold approximation and projection; ZO-1, Zona occludens 1.

Financial support

Health and Medical Research Fund (03143476) and the Innovation and Technology Fund, University-Industry Collaboration Programme (UIM/300), the Government of the Hong Kong Special Administrative Region to PKHT. Seed Funding for Basic Research, The University of Hong Kong (201611159160 & 201711159135) to VCHL. Sanming Project of Medicine in Shenzhen, China (SZSM201812055) to BW. National Natural Science Foundation of China (81771629) to HX.

Conflict of interest

The authors declare no conflicts of interest that pertain to this work.

Please refer to the accompanying ICMJE disclosure forms for further details.

Authors' contributions

RO Babu: Experimentation, data acquisition, bioinformatics analysis, manuscript writing. VCH Lui: Experimentation, project

organoid. For a complete gene list, see Table S4. (C) Heatmap showing the mRNA expression levels of total DEGs (n = 6,495) in beta-amyloid-treated when compared to untreated control organoids. (D) Boxplot for the mRNA expression levels of topmost hepatobiliary genes in beta-amyloid-treated *vs.* untreated control organoids at p <0.05 (2-tailed Student's t test). (E) Boxplot for the mRNA expression levels of topmost beta-amyloid pathway-related genes in beta-amyloid-treated and untreated control organoids at p <0.05 (2-tailed Student's t test). (F) Venn diagram of DEGs involved in the beta-amyloid pathway in organoids derived from patients with BA (Fig. S9) *vs.* beta-amyloid-treated organoids (Fig. S15). BA, biliary atresia; DEGs, differentially expressed genes; UMAP, uniform manifold approximation and projection. (This figure appears in color on the web.)

planning, data acquisition and analysis, manuscript writing. Y Chen & RSW Yiu: Experimentation, data acquisition and analysis. Y Ye; MON Yu; PHY Chung; KKY Wong; H Xia: & B Wang: Patient recruitment, liver biopsy, data acquisition and analysis. B Niu: Bioinformatic analysis. Z Wu: Date acquisition. R Zhang: Patient recruitment, data acquisition and analysis. MQ Zhang: Bioinformatic analysis and *in silico* experiment planning. U Lendahl & PKH Tam: Project planning, data acquisition and analysis, manuscript writing.

Acknowledgements

The authors thank all the patients participated in this study; HKU CPOS for sequencing service; QMH EMU for TEM study; Hans Clevers for the help in the establishment of liver organoids. This work is supported by HMRF (03143476) and ITF-UICP (UIM/300), HKSAR Government to PKHT; the Seed-Funding for Basic Research, HKU (201611159160 & 201711159135) to VCHL; Sanming Project of Medicine in Shenzhen, China (SZSM2018 12055) to BW; National Natural Science Foundation of China (81771629) to HX.

Supplementary data

Supplementary data to this article can be found online at https://doi.org/10.1016/j.jhep.2020.06.012.

References

[1] Tam PKH, Yiu RS, Lendahl U, Andersson ER. Cholangiopathies - towards a molecular understanding. EBioMedicine 2018;35:381–393.
[2] Sanchez-Valle A, Kassira N, Varela VC, Radu SC, Paidas C, Kirby RS. Biliary atresia: epidemiology, genetics, clinical update, and public health perspective. Adv Pediatr 2017;64:285–305.
[3] Hartley JL, Davenport M, Kelly DA. Biliary atresia. Lancet 2009;374:1704–1713.
[4] Tam PKH, Chung PHY, St Peter SD, Gayer CP, Ford HR, Tam GCH, et al. Advances in paediatric gastroenterology. Lancet 2017;390:1072–1082.
[5] Feldman AG, Sokol RJ. Neonatal cholestasis: emerging molecular diagnostics and potential novel therapeutics. Nat Rev Gastroenterol Hepatol 2019;16:346–360.
[6] Girard M, Panasyuk G. Genetics in biliary atresia. Curr Opin Gastroenterol 2019;35:73–81.
[7] Garcia-Barcelo MM, Yeung MY, Miao XP, Tang CS, Cheng G, So MT, et al. Genome-wide association study identifies a susceptibility locus for biliary atresia on 10q24.2. Hum Mol Genet 2010;19:2917–2925.
[8] Leyva-Vega M, Gerfen J, Thiel BD, Jurkiewicz D, Rand EB, Pawlowska J, et al. Genomic alterations in biliary atresia suggest region of potential disease susceptibility in 2q37.3. Am J Med Genet A 2010;152A:886–895.
[9] Cheng G, Tang CS, Wong EH, Cheng WW, So MT, Miao X, et al. Common genetic variants regulating ADD3 gene expression alter biliary atresia risk. J Hepatol 2013;59:1285–1291.
[10] Chen Y, Gilbert MA, Grochowski CM, McEldrew D, Llewellyn J, Waisbourd-Zinman O, et al. A genome-wide association study identifies a susceptibility locus for biliary atresia on 2p16.1 within the gene EFEMP1. Plos Genet 2018;14:e1007532.
[11] Berauer JP, Mezina AI, Okou DT, Sabo A, Muzny DM, Gibbs RA, et al. Identification of polycystic kidney disease 1 like 1 gene variants in children with biliary atresia splenic malformation syndrome. Hepatology 2019;70:899–910.
[12] Riepenhoff-Talty M, Schaekel K, Clark HF, Mueller W, Uhnoo I, Rossi T, et al. Group A rotaviruses produce extrahepatic biliary obstruction in orally inoculated newborn mice. Pediatr Res 1993;33:394–399.
[13] Huch M, Gehart H, van Boxtel R, Hamer K, Blokzijl F, Verstegen MM, et al. Long-term culture of genome-stable bipotent stem cells from adult human liver. Cell 2015;160:299–312.
[14] Huch M, Dorrell C, Boj SF, van Es JH, Li VS, van de Wetering M, et al. In vitro expansion of single Lgr5+ liver stem cells induced by Wnt-driven regeneration. Nature 2013;494:247–250.
[15] Andersson ER, Chivukula IV, Hankeova S, Sjoqvist M, Tsoi YL, Ramskold D, et al. Mouse model of Alagille syndrome and mechanisms of Jagged1 Missense mutations. Gastroenterology 2018;154:1080–1095.
[16] Boj SF, Vonk AM, Statia M, Su J, Vries RR, Beekman JM, et al. Forskolin-induced swelling in intestinal organoids: an in vitro assay for assessing drug response in cystic fibrosis patients. J Vis Exp 2017:55159.
[17] Gigliozzi A, Fraioli F, Sundaram P, Lee J, Mennone A, Alvaro D, et al. Molecular identification and functional characterization of Mdr1a in rat cholangiocytes. Gastroenterology 2000;119:1113–1122.
[18] Mizutani T, Nakamura T, Morikawa R, Fukuda M, Mochizuki W, Yamauchi Y, et al. Real-time analysis of P-glycoprotein-mediated drug transport across primary intestinal epithelium three-dimensionally cultured in vitro. Biochem Biophys Res Commun 2012;419:238–243.
[19] Martin-Belmonte F, Perez-Moreno M. Epithelial cell polarity, stem cells and cancer. Nat Rev Cancer 2011;12:23–38.
[20] Picelli S, Bjorklund AK, Faridani OR, Sagasser S, Winberg G, Sandberg R. Smart-seq2 for sensitive full-length transcriptome profiling in single cells. Nat Methods 2013;10:1096–1098.
[21] Ober EA, Lemaigre FP. Development of the liver: insights into organ and tissue morphogenesis. J Hepatol 2018;68:1049–1062.
[22] Zong Y, Stanger BZ. Molecular mechanisms of bile duct development. Int J Biochem Cell Biol 2011;43:257–264.
[23] Yoo KS, Lim WT, Choi HS. Biology of cholangiocytes: from bench to bedside. Gut Liver 2016;10:687–698.
[24] Aizarani N, Saviano A, Sagar, Mailly L, Durand S, Herman JS, et al. A human liver cell atlas reveals heterogeneity and epithelial progenitors. Nature 2019;572:199–204.
[25] Yamada M, Sodeyama N, Itoh Y, Suematsu N, Otomo E, Matsushita M, et al. A deletion polymorphism of alpha(2)-macroglobulin gene and cerebral amyloid angiopathy. Stroke 1999;30:2277–2279.
[26] Wyatt AR, Constantinescu P, Ecroyd H, Dobson CM, Wilson MR, Kumita JR, et al. Protease-activated alpha-2-macroglobulin can inhibit amyloid formation via two distinct mechanisms. FEBS Lett 2013;587:398–403.
[27] Varma VR, Varma S, An Y, Hohman TJ, Seddighi S, Casanova R, et al. Alpha-2 macroglobulin in Alzheimer's disease: a marker of neuronal injury through the RCAN1 pathway. Mol Psychiatry 2017;22:13–23.
[28] Davies J, Zachariades E, Rogers-Broadway KR, Karteris E. Elucidating the role of DEPTOR in Alzheimer's disease. Int J Mol Med 2014;34:1195–1200.
[29] Lanoiselee HM, Nicolas G, Wallon D, Rovelet-Lecrux A, Lacour M, Rousseau S, et al. APP, PSEN1, and PSEN2 mutations in early-onset Alzheimer disease: a genetic screening study of familial and sporadic cases. Plos Med 2017;14:e1002270.
[30] Castellano JM, Kim J, Stewart FR, Jiang H, DeMattos RB, Patterson BW, et al. Human apoE isoforms differentially regulate brain amyloid-beta peptide clearance. Sci Transl Med 2011;3:89ra57.
[31] O'Brien RJ, Wong PC. Amyloid precursor protein processing and Alzheimer's disease. Annu Rev Neurosci 2011;34:185–204.
[32] Lertudomphonwanit C, Mourya R, Fei L, Zhang Y, Gutta S, Yang L, et al. Large-scale proteomics identifies MMP-7 as a sentinel of epithelial injury and of biliary atresia. Sci Transl Med 2017;9:eaan8462.
[33] Dunys J, Valverde A, Checler F. Are N- and C-terminally truncated Abeta species key pathological triggers in Alzheimer's disease? J Biol Chem 2018;293:15419–15428.
[34] Benveniste O, Stenzel W, Hilton-Jones D, Sandri M, Boyer O, van Engelen BG. Amyloid deposits and inflammatory infiltrates in sporadic inclusion body myositis: the inflammatory egg comes before the degenerative chicken. Acta Neuropathol 2015;129:611–624.
[35] Hansen D, Ling H, Lashley T, Holton JL, Warner TT. Review: Clinical, neuropathological and genetic features of Lewy body dementias. Neuropathol Appl Neurobiol 2019;45:635–654.
[36] Tyraskis A, Davenport M. Steroids after the Kasai procedure for biliary atresia: the effect of age at Kasai portoenterostomy. Pediatr Surg Int 2016;32:193–200.
[37] Schreiber RA, Barker CC, Roberts EA, Martin SR, Alvarez F, Smith L, et al. Biliary atresia: the Canadian experience. J Pediatr 2007;151:659–665. 665.e1.
[38] Nio M, Wada M, Sasaki H, Tanaka H. Effects of age at Kasai portoenterostomy on the surgical outcome: a review of the literature. Surg Today 2015;45:813–818.
[39] Zahm AM, Hand NJ, Boateng LA, Friedman JR. Circulating microRNA is a biomarker of biliary atresia. J Pediatr Gastroenterol Nutr 2012;55:366–369.
[40] Peng X, Yang L, Liu H, Pang S, Chen Y, Fu J, et al. Identification of circulating MicroRNAs in biliary atresia by next-generation sequencing. J Pediatr Gastroenterol Nutr 2016;63:518–523.

[41] Dong R, Shen Z, Zheng C, Chen G, Zheng S. Serum microRNA microarray analysis identifies miR-4429 and miR-4689 are potential diagnostic biomarkers for biliary atresia. Scientific Rep 2016;6:21084.
[42] Yang L, Zhou Y, Xu PP, Mourya R, Lei HY, Cao GQ, et al. Diagnostic accuracy of serum matrix metalloproteinase-7 for biliary atresia. Hepatology 2018;68:2069–2077.
[43] Kaushik A, Jayant RD, Tiwari S, Vashist A, Nair M. Nano-biosensors to detect beta-amyloid for Alzheimer's disease management. Biosens Bioelectron 2016;80:273–287.
[44] Waisbourd-Zinman O, Koh H, Tsai S, Lavrut PM, Dang C, Zhao X, et al. The toxin biliatresone causes mouse extrahepatic cholangiocyte damage and fibrosis through decreased glutathione and SOX17. Hepatology 2016;64:880–893.
[45] Lorent K, Gong W, Koo KA, Waisbourd-Zinman O, Karjoo S, Zhao X, et al. Identification of a plant isoflavonoid that causes biliary atresia. Sci Transl Med 2015;7:286ra267.
[46] Thakurdas SM, Lopez MF, Kakuda S, Fernandez-Valdivia R, Zarrin-Khameh N, Haltiwanger RS, et al. Jagged1 heterozygosity in mice results in a congenital cholangiopathy which is reversed by concomitant deletion of one copy of Poglut1 (Rumi). Hepatology 2016;63:550–565.